Acta Astronautica 173 (2020) 69–75

Contents lists available at ScienceDirect

Acta Astronautica

journal homepage: www.elsevier.com/locate/actaastro

Study and modeling of propellant ablation in coaxial ablative pulsed plasma thrusters

Tiankun Huang[a], Zhiwen Wu[a,*], Guorui Sun[b], Xiangyang Liu[a], William Yeong Liang Ling[a]

[a] School of Aerospace Engineering, Beijing Institute of Technology, Beijing, 100081, PR China
[b] Tianjin Institute of Power Sources, Tianjin, 300384, PR China

ARTICLE INFO

Keywords:
Ablative pulsed plasma thruster
Coaxial electrodes
Propellant ablation
Modeling

ABSTRACT

The influence of the main design parameters on the ablated mass bit (the mass ablated from the propellant in each discharge) of a coaxial ablative pulsed plasma thruster is analyzed in this paper. The analysis results show that the main influencing factor of the ablated mass bit in coaxial ablative pulsed plasma thrusters is the ablation energy from the arc. When the ablation energy is given, the shape and size of the propellant surface mainly affect the distribution of the ablated mass but have less influence on the ablated mass bit. Based on the analysis, a simple model that can be used to estimate the ablated mass bit of the coaxial ablative pulsed plasma thruster is established. To evaluate and complete the new model, a coaxial ablative pulsed plasma thruster is operated and tested under 10 different working conditions. The experimental results show that the ratio of the ablated mass bit to the absolute value integrals of the product of the electrode voltage and discharge current is approximately 0.38–0.49 μg/J. When the ratio is set to 0.44 μg/J, the maximum and average errors of the new model are 15.7% and 7.6%, respectively, for ablated mass bits under these 10 working conditions. The concept of the ablation direction is proposed in this paper. The experimental and simulation results show that the ablation direction has a great influence on the propellant surface profile change in coaxial ablative pulsed plasma thrusters, which also affects their performance and reliability.

1. Introduction

The small satellite market has grown rapidly in recent years [1]. It is estimated that in the next 3 years, more than 300 small satellites will be launched [2]. To increase the orbit control ability and lifetime of the small satellites, micropropulsion systems are needed [3]. These propulsion systems must satisfy the small volume, light weight, low power, total impulse, and low cost requirements [4].

As the first electric propulsion system applied to the spacecraft mission [5], the ablative pulsed plasma thruster (APPT) is suitable for small satellite propulsion missions [6,7]. Compared to cold gas and chemical propulsions, the APPT has a high specific impulse (the impulse produced by a unit mass of propellant) and can reduce the total propellant mass [3]. Additionally, compared to other electric propulsions (such as Hall and ion thrusters), the APPT features a simple structure, high reliability and low power consumption [8–10].

APPTs can be divided into two types: the parallel-plate type and the coaxial type [5]. Coaxial APPTs are competitive in the micropropulsion field because coaxial electrode structures have great advantages with respect to miniaturization [11]. In recent years, the coaxial APPT has been the focus of small satellite designers and some small satellites [12–14] using coaxial APPTs have been launched.

The propellant of an APPT is usually Teflon. Fig. 1 shows the schematic of a coaxial APPT [15]. The capacitor is used to store discharge energy. The igniter plug produces the initial plasma to trigger the capacitor discharge. The arc ablates the solid propellant to produce neutral gas, which can be ionized and become plasma in a high-voltage electric field. The plasma can maintain the discharge and be accelerated by the pressure and electromagnetic forces to generate thrust.

Propellant ablation is an important physical process that has a great influence on the performance and reliability of an APPT. For a parallel-plate APPT, many experimental results have demonstrated the effects of the design parameters on the ablated mass bit (the ablated mass produced by a single discharge) [16]. In addition, many ablation models based on the parallel-plate APPT have also been established for estimating the ablated mass or studying ablation mechanisms [17,18].

The ablation mechanism of a coaxial APPT is more complex than that of a parallel-plate APPT because the distributions of the current density and electric field above its propellant surface are nonuniform in the radial direction [19,20]. During the past 20 years, some

* Corresponding author.
E-mail address: bitwzw@bit.edu.cn (Z. Wu).

https://doi.org/10.1016/j.actaastro.2020.04.010
Received 25 February 2020; Received in revised form 6 April 2020; Accepted 8 April 2020
Available online 14 April 2020

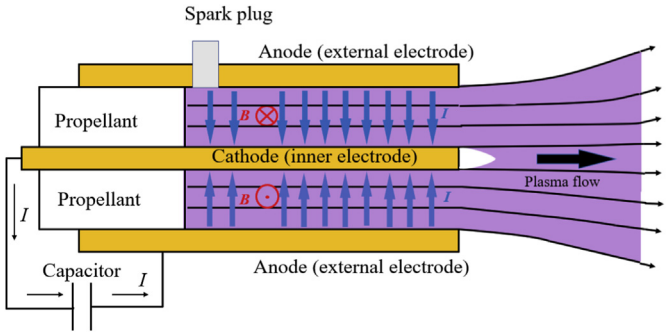

Fig. 1. Schematic of a coaxial APPT.

experimental results regarding the ablation of coaxial APPTs were obtained and analyzed. The important studies are as follows.

In 2002, Gregory G. Spanjers developed a coaxial microAPPT and measured its ablated mass bit and propellant temperature [21]. The ablated mass bit of the APPT was approximately constant over 90 h of discharge (1 Hz). Based on a coaxial microAPPT, Michael Keidar discussed the optimization issues of a coaxial APPT [22]. According to his analysis, the choice of discharge energy is very important. A small energy may lead to serious propellant charring, and large energy may cause another circumferential discharge nonuniformity or arc spoking. In addition, Michael Keidar also developed a Teflon ablation model to study the radial nonuniformity of the coaxial PPT ablation rate [23].

However, past studies of the propellant ablation in coaxial APPTs have been focused on the charring or nonuniformity phenomenon. Studies on the relationship between the ablated mass bit and design parameters (such as the propellant size and capacitor initial voltage) are deficient. The ablated mass bit has a great effect on the APPT performance, and this deficiency goes against the designs and optimizations of coaxial APPTs. In addition, a model that can estimate the ablated mass bit of a coaxial APPT is also needed to evaluate design schemes.

Therefore, the relationship between the main design parameters and ablated mass bit in a coaxial APPT is analyzed in this paper. Based on the analysis, a simple model is established for rapidly estimating the ablated mass bit of a coaxial APPT. In addition, a series of experiments are carried out to evaluate and complete the model. Finally, the model error and the evolution process of the coaxial APPT propellant surface are analyzed.

2. Analysis and modeling of propellant ablation in coaxial APPTs

For a coaxial APPT using Teflon propellant, the main ablation influence factors are the propellant external diameter, the propellant inner diameter and the discharge circuit parameters (resistance, inductance, capacitance and capacitor initial voltage). To simplify the model, the discharge product deposition [7] is neglected.

Here, the surface of a coaxial PPT propellant is divided into a series of narrow ring surfaces, shown in Fig. 2. The thicknesses of these surfaces are δ (δ is infinitesimal).

According to Joule's law, at time t, the electric power on the ring surface of radius r can be computed by:

$$P_e(r, t) = |I(t)E(r, t)|\delta \tag{1}$$

where $I(t)$ is the discharge current and $E(r, t)$ is the electric field intensity at the position where r is distance from the propellant center.

As the energy for PPT propellant ablation comes from the arc [5], the propellant ablation rate has a positive correlation relationship with the electric power above the propellant surface. Thus, on the ring surface of radius r, the propellant ablation rate can be computed as follow:

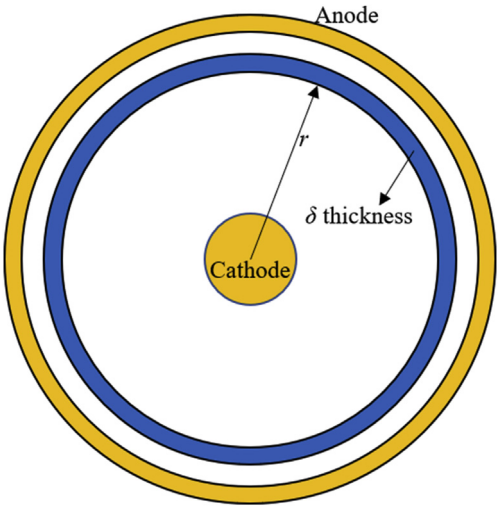

Fig. 2. Diagram of a narrow ring surface.

$$v_a(r, t) \propto p_e(r, t) = \frac{P_e(r, t)}{2\pi r\delta} = \left|\frac{I(t)E(r, t)}{2\pi r}\right| \tag{2}$$

where $v_a(r, t)$ and $p_e(r, t)$ are the ablation rate and the electric power per unit area on the ring surface of radius r, respectively.

In the ablation model in this paper, it is assumed that $v_a(r, t)$ is proportional to $p_e(r, t)$ and the coefficient is constant and represented as α.

Thus, (2) can be written by:

$$v_a(r, t) = \alpha\left|\frac{I(t)E(r, t)}{2\pi r}\right| \tag{3}$$

For a coaxial electric field, the electric field intensity is computed by:

$$E(r, t) = \frac{U(t)}{r\ln\left(\frac{r_2}{r_1}\right)} \tag{4}$$

where r_1 and r_2 are the inner radius and external radius of the propellant surface, respectively, and $U(t)$ is the electrode voltage.

Based on (3) and (4), the ablation rate is computed by:

$$v_a(r, t) = \frac{\alpha|U(t)I(t)|}{2\pi r^2\ln\left(\frac{r_2}{r_1}\right)} \tag{5}$$

Based on (5), the ablation depth at the position r from the propellant center after a single discharge can be computed by:

$$d(r) = \frac{\int_0^{t_1} v_a(r, t)dt}{\rho} = \frac{\alpha\int_0^{t_1}|U(t)I(t)|dt}{2\pi\rho r^2\ln\left(\frac{r_2}{r_1}\right)} \tag{6}$$

where ρ is the propellant density and t_1 is the time when a PPT discharge ends.

Based on (5), the ablated mass bit can be computed by:

$$m = \int_0^{t_1}\int_{r_1}^{r_2} 2\pi r v_a(r, t)drdt = = \int_0^{t_1}\alpha|U(t)I(t)|dt \tag{7}$$

According to (6), from the external electrode to the inner electrode, the ablation depth increases. An obvious concavity appears on the coaxial APPT propellant surface. This phenomenon has been proven by past research [23]. On the other hand, the absolute value integral of the product of the electrode voltage and discharge current is actually the total electric energy flowing between the electrodes, whose value is determined by the discharge circuit parameter. Therefore, it can be concluded that the ablated mass bit is only affected by the discharge circuit parameters according to (7). The shape and size of the propellant

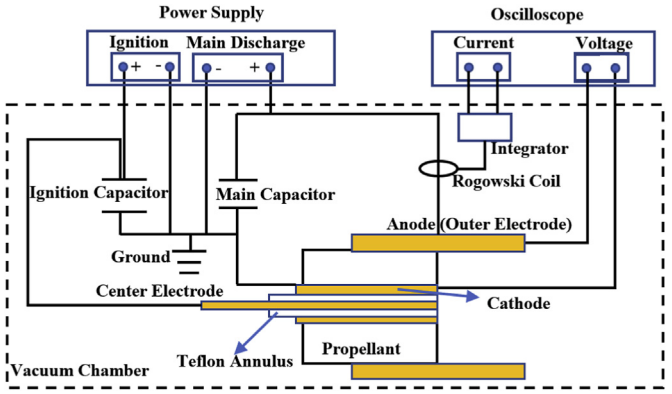

Fig. 3. Schematic of the three-electrode coaxial APPT and test system.

surface mainly affect the distribution of the ablated mass. The coefficient α will be obtained according to the experimental results in section 3.

3. Experiments for developing and evaluating the model

3.1. Experimental setup

3.1.1. Thruster heads

In this research, the three-electrode coaxial structure [21] is adopted (shown in Fig. 3). The center electrode is used to produce the initial plasma for triggering the main discharge. Five different thruster heads are prepared. The diameters of these heads are 7 mm, 8 mm, 9 mm, 10 mm and 11 mm. The five thruster heads use the same center electrode, cathode (1.5 mm outer diameter), and Teflon annulus. The anode wall thicknesses of these heads are 0.5 mm.

3.1.2. Transmission conductors

Two discharge circuits are used in this study. In Circuit 1, coaxial wires are used as transmission conductors to connect the electrodes and capacitor. In Circuit 2, metal sheets are used to replace some coaxial wires to reduce the total resistance and inductance of the discharge circuit.

3.1.3. Test system

The APPTs work in a vacuum chamber that can provide a 5×10^{-3} Pa discharge environment. The electrode voltage and discharge current are measured by a high-voltage probe (Tektronix THDP0100) and a Rogowski coil (CWT MiniHF 150R), respectively. The ablated mass is obtained by a high-precision balance (Sartorius CPA225D). The performances of the high-voltage probe, the Rogowski coil and the high-precision balance are shown in Tables 1–3, respectively. The test system is shown in Fig. 3. The sampling rate of the oscilloscope is 2.5 GS/s.

3.2. Procedures

Ten working conditions are selected (shown in Table 4). For each condition, the APPT works 2000 times (1 Hz frequency). After 2000 discharges, the mass loss of the propellant block is measured, and the ablated mass bit is calculated by dividing the propellant mass loss by the discharge number. The discharge current and electrode voltage are also measured and analyzed. The absolute value integral of the product of the electrode voltage and discharge current is calculated for obtaining the coefficient α.

Table 1
Performance of the high-voltage probe.

Parameters	Values
Bandwidth	100 MHz
Maximum input	2300 V
Rising time	< 3.5 ns
Length of cables	1.5 m

Table 2
Performance of the Rogowski coil.

Parameters	Values
Bandwidth	12 MHz
Maximum input	30 kA
Accuracy	< 0.2%
Length of cables	1 m

Table 3
Performance of the high-precision balance.

Parameters	Values
Maximum input	100 g
Readability	0.01 mg
Standard deviation	0.05 mg
Linearity	0.1 mg

Table 4
The working conditions selected in this study.

Number	Initial Voltage	Capacitor	Circuit	Head Diameter
1	800 V	2 μF	1	7 mm
2	1000 V	2 μF	1	7 mm
3	1200 V	2 μF	1	7 mm
4	1400 V	2 μF	1	7 mm
5	1500 V	2 μF	1	7 mm
6	1400 V	2 μF	2	7 mm
7	1400 V	2 μF	2	8 mm
8	1400 V	2 μF	2	9 mm
9	1400 V	2 μF	2	10 mm
10	1400 V	2 μF	2	11 mm

4. Results and discussion

The electrode voltage and discharge current waveforms under the working conditions 1–5 are shown in Fig. 4. Under these operating conditions, the PPT worked under different capacitor initial voltages (800 V, 1000 V, 1200 V, 1400 V, and 1500 V) and Circuit 1.

The PPT worked under operating conditions 6–10. Under these operating conditions, the PPT worked with different propellant external diameters (6 mm, 7 mm, 8 mm, 9 mm, and 10 mm) and Circuit 2. The electrode voltage and discharge current waveforms are shown in Fig. 5.

As the discharge circuit of an APPT can be regarded as a resistor-inductor-capacitor (RLC) circuit, the total resistance and inductance of the circuit can be estimated according to the discharge current waveform [24,25]. According to Figs. 4 and 5, the total resistance and inductance of Circuit 2 are approximately 50 mΩ and 99 nH, respectively, and the total resistance and inductance of Circuit 1 are approximately 91 mΩ and 128 nH, respectively. The transmission conductors in Circuit 1 consume more discharge energy.

The average ablated mass bits under working conditions 1–10 are shown in Tables 5 and 6. Based on (7), the coefficients α under working conditions 1–10 are calculated, and the results are also shown in Tables 5 and 6

It can be seen that the coaxial APPT has a higher ablated mass bit with a higher initial discharge energy or less electric energy loss. Even if the working conditions are different, the coefficients α are close. These coefficients α range from 0.38 μg/J to 0.49 μg/J.

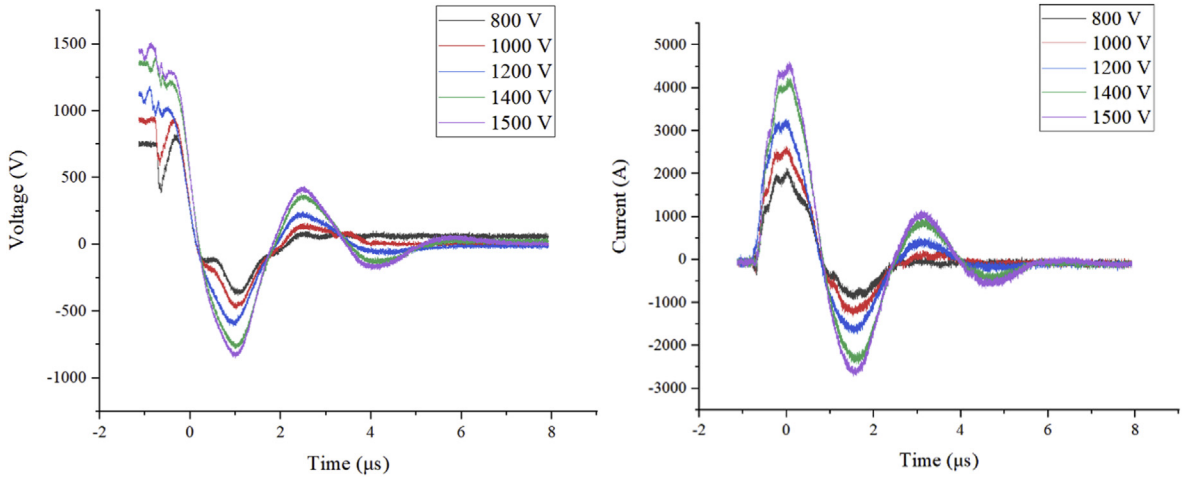

Fig. 4. Electrode voltage and discharge current waveforms under the working conditions 1–5.

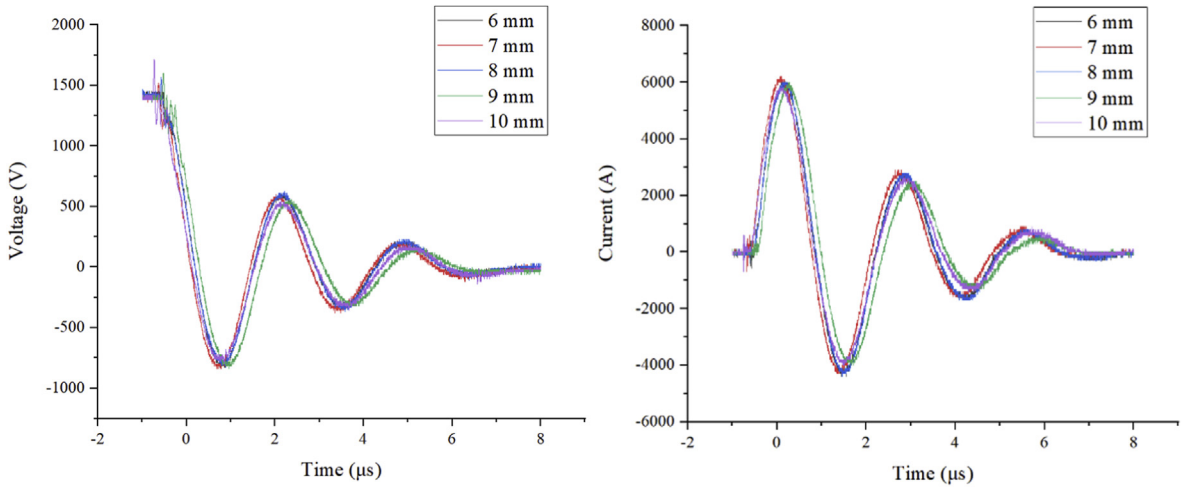

Fig. 5. Electrode voltage and discharge current waveforms under the operating conditions 6–10.

Table 5
The average ablated mass bits under working conditions 1–5.

Condition	1	2	3	4	5
Ablated mass bit (μg)	0.72 ± 0.03	1.13 ± 0.03	1.66 ± 0.03	2.31 ± 0.03	2.73 ± 0.03
Coefficient α (μg/J)	0.40 ± 0.02	0.49 ± 0.02	0.44 ± 0.01	0.46 ± 0.01	0.46 ± 0.01

Table 6
The average ablated mass bits under working conditions 6–10.

Condition	6	7	8	9	10
Ablated mass bit (μg)	3.10 ± 0.03	2.53 ± 0.03	2.48 ± 0.03	2.74 ± 0.03	3.09 ± 0.03
Coefficient α (μg/J)	0.48 ± 0.01	0.39 ± 0.01	0.38 ± 0.01	0.43 ± 0.01	0.48 ± 0.01

4.1. Model evaluation

4.1.1. The results of the ablated mass bit estimation

The average value of the coefficients α in Table 2 is 0.44 μg/J. Based on (7) in this paper, the simulation results of the ablated mass bits under the 10 working conditions are shown in Fig. 6.

The results in Fig. 6 show that the maximum and average errors of the model in this paper are 15.7% and 7.6%, respectively, when the coefficients α is set to 0.44 μg/J. The error of the new model mainly comes from neglecting the deposition of discharge products. According to past studies [22], a part of discharge products deposit on the propellant surface and affect the ablated mass bit of an APPT.

4.1.2. The results of the evolution of the propellant surface

The coefficient α is set to 0.44 μg/J. Based on the model in this paper, under condition 6, the ablation depth distributions of the propellant surface after 1 discharge, 2000 discharges, 20,000 discharges and 54,000 discharges are shown in Fig. 7.

Fig. 7 shows that an obvious concavity gradually forms on the propellant surface as the discharge number increases. According to past studies [26], an APPT cannot discharge if the included angle between the propellant surface and electrodes is too small. Therefore, the coaxial

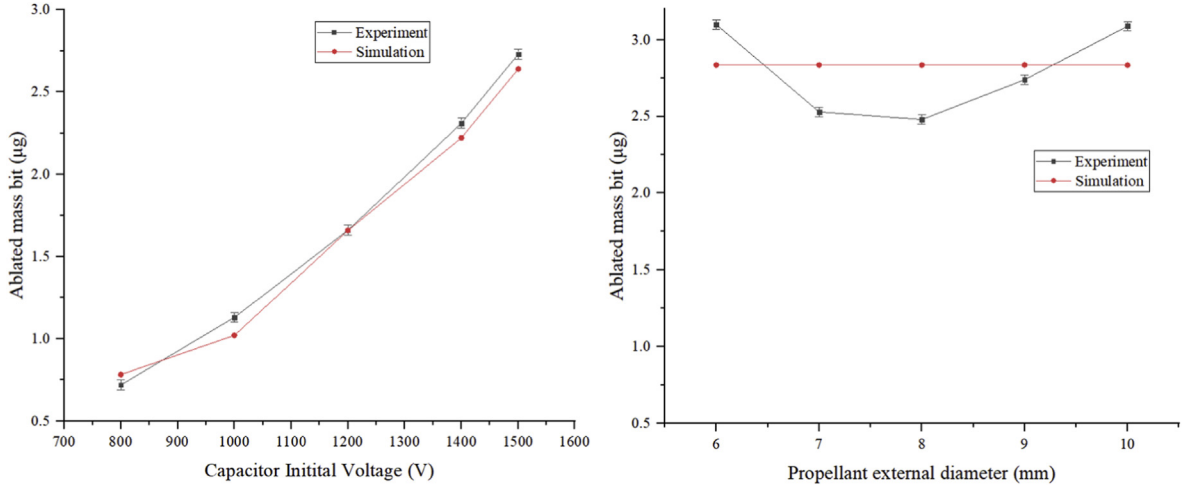

Fig. 6. Comparison of the simulation and experimental results.

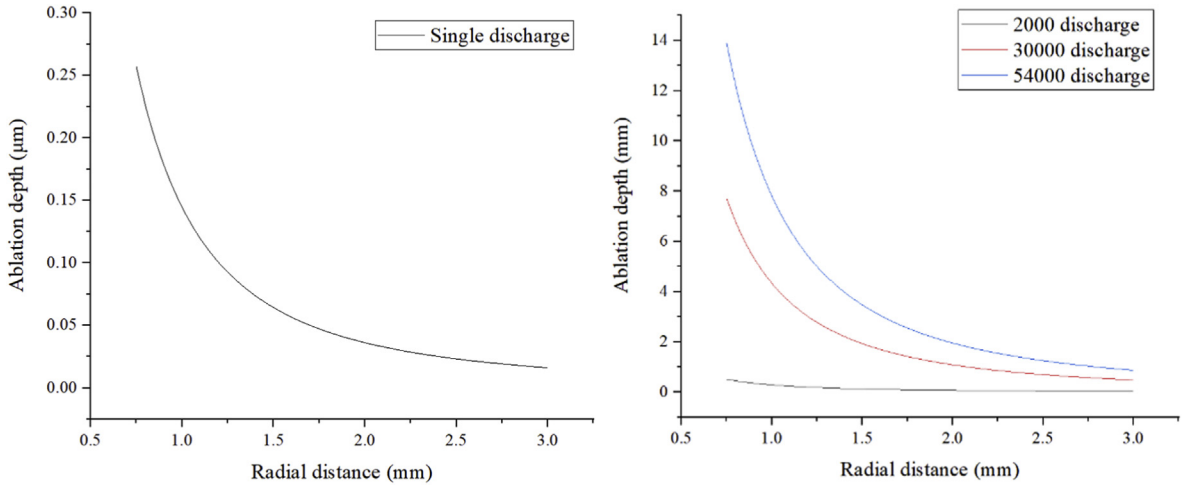

Fig. 7. The simulation results of the ablation depth distributions.

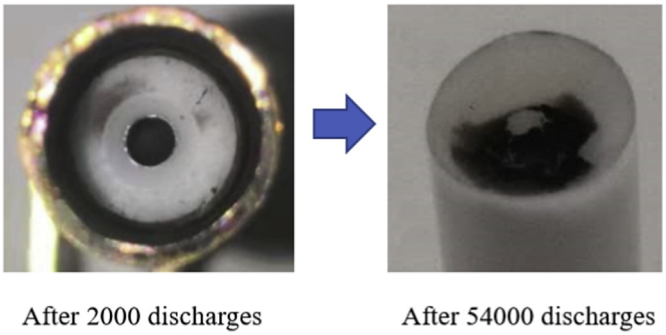

Fig. 8. Photographs of the propellant surfaces after 2000 discharges and 54,000 discharges (condition 6).

APPT cannot work before 20,000 discharges under condition 6 because the ablation depth near the inner electrode has exceeded the propellant outer diameter (6 mm). However, the experimental result is opposite to the simulation result. The coaxial APPT can work more than 54,000 times under condition 6. Photographs of the propellant surfaces after 2000 discharges and 54,000 discharges are shown in Fig. 8.

It is shown that the simulation result and the experimental result are relatively close after 2000 discharges. However, the propellant surface changes to a bowl shape, which has also been observed in previous studies [21].

Some researchers think that the radial nonuniformity of the ablation rate leads to the bowl-shaped propellant surface of a coaxial APPT. However, the results in this study show that radial nonuniformity is not the only reason. If the propellant ablation rate near the inner electrode is always much higher than that near the outer electrode, then the concave depth of the propellant surface would be very large when the discharge number is high, and the obvious profile change shown in Fig. 8 cannot occur.

The other important reason that leads to the bowl-shaped surface is radial ablation. In past studies of APPTs, the ablation directions on the propellant surface are considered to be consistent and parallel to the electrodes. This view is basically correct for parallel-pate APPTs because their propellant surfaces are approximately perpendicular to electrodes at all times. However, for a coaxial APPT, the ablation directions on the propellant surface are not consistent after the first discharge.

The experimental results shown in Fig. 8 can be explained by the results in Fig. 9.

(1) When the discharge number is very low, the propellant surface can be regarded as a plane. As the ablation rate is relatively higher near the center, an obvious concavity gradually forms as the discharge number increases.
(2) As the profile of the propellant surface changes, the radial (y direction shown in Fig. 9) ablation cannot be neglected. From the

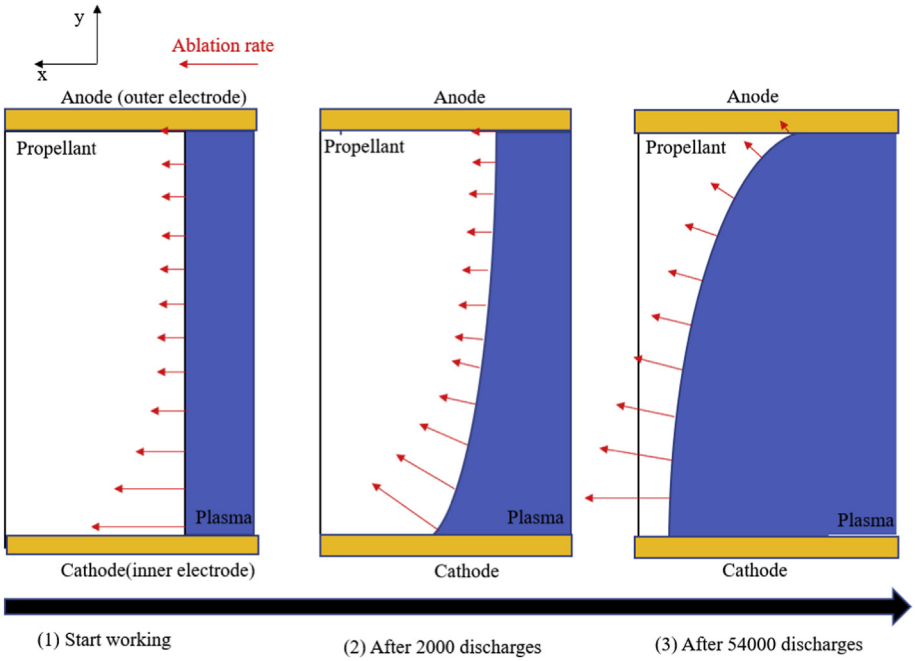

Fig. 9. Analysis of the propellant surface evolution shown in Fig. 8.

external electrode to the inner electrode, the proportion of the radial ablation rate increases. The radial ablation greatly reduces the axial ablation rate near the inner electrode and prevents discharge failure of the APPT.

(3) Due to the effects of axial and radial ablations, the propellant surface of the APPT forms a bowl shape after 54,000 discharges. Consistent with the ablation rate distribution on the surface, the shape change should continue.

According to the analysis in section 2, the profile change in the propellant surface has little effect on the ablated mass bit of a coaxial APPT if the ablation energy is constant. This conjecture can be proven by the experimental results in reference 19. The propellant surface profile mainly affects the distribution of the ablated mass. Therefore, the model in this paper can also be used when the discharge number is high. Of course, the shape change of the propellant surface in coaxial APPTs should be studied because it could affect the plasma acceleration and discharge reliability.

The propellant surface evolution of the coaxial APPT will be modeled in future studies. Besides adding the computations for the radial ablation, the grid resolution of the propellant surface and the number of steps should be set to suitable values for reducing the accumulated error [27,28].

5. Conclusion and outlook

The relationship between the ablated mass bit and the main design parameters in coaxial ablative pulsed plasma thrusters is analyzed in this paper. Based on the analysis, a simple model for estimating the ablated mass bit of a coaxial ablative pulsed plasma thruster is established. To evaluate the model and obtain an important coefficient in the model, a coaxial ablative pulsed plasma thruster is operated and tested under various working conditions. In addition, the propellant surface evolution in a coaxial ablative pulsed plasma thruster is also discussed based on the simulation and experimental results in this paper. The main conclusions are as follows:

(1) The main influencing factor of the ablated mass bit in a coaxial ablative pulsed plasma thruster is the ablation energy from the arc. When the ablation energy is given, the shape and size of the propellant surface mainly affect the distribution of the ablated mass but have less influence on the ablated mass bit.

(2) The experimental results show that the ratio of the ablated mass bit to the absolute value integrals of the product of the electrode voltage and discharge current is approximately 0.38–0.49 μg/J. When the ratio is set to 0.44 μg/J in the model in this paper, the model maximum and average errors are 15.7% and 7.6%, respectively, for estimating the ablated mass bit.

(3) When the discharge number is relativity high, the new model cannot be used to obtain the ablated mass distribution of the propellant surface in a coaxial ablative pulsed plasma thruster at present because the ablation direction is neglected. However, this neglect would not reduce the accuracy of the new model for the ablated mass bit estimation because the ablation direction does not affect the value of the total ablated mass.

(4) The propellant surface is not a constant shape and will change over the entire life of a coaxial ablative pulsed plasma thruster because of the effects of axial and radial ablations. The shape change may influence the performance and reliability of a coaxial ablative pulsed plasma thruster and should be studied in the future.

The analysis and experimental results in this paper provide references for the design and optimization of coaxial ablative pulsed plasma thrusters. The new ablation model can be used to rapidly estimate the ablated mass bit of a coaxial ablative pulsed plasma thruster. The ability and accuracy of this model could be improved by adding the computations for the radial ablation and the discharge product deposition [7] in the future.

Declaration of competing interest

The authors declare that there is no conflict of interest between this article and others. The authors declare that they have no known competing financial interests or personal relationships that could have appeared to influence the work reported in this paper.

Acknowledgments

This research was supported by National Natural Science Foundation of China (11672039).

References

[1] Dan Lev, et al., The technological and commercial expansion of electric propulsion, Acta Astronaut. 159 (2019) 213–227.
[2] Carlos Niederstrasser, Northrop Grumman Corporation, Small launch vehicles - a 2018 state of the industry survey, Proceedings of the 32nd Annual AIAA/USU Conference on Small Satellites, Logan, UT, USA, 2018.
[3] Kristina Lemmer, Propulsion for CubeSats, Acta Astronaut. 134 (2017) 231–243.
[4] Dan Lev, et al., The technological and commercial expansion of electric propulsion in the past 24 years, Proceedings of the 35th International Electric Propulsion Conference, Atlanta, Georgia, Logan, USA, 2017.
[5] R.L. Burton, P.J. Turchi, Pulsed plasma thruster, J. Propul. Power 14 (5) (1998) 716–734.
[6] M.V. Silnikov, et al., Correction thruster development based on high-current surface discharge in vacuum, Acta Astronaut. 109 (2015) 177–181.
[7] Tiankun Huang, et al., Study of breakdown in an ablative pulsed plasma thruster, Phys. Plasmas 22 (2015) 103511.
[8] S. Ciaralli, et al., Results of the qualification test campaign of a pulsed plasma thruster for cubesat propulsion (PPTCUP), Acta Astronaut. 121 (2016) 314–322.
[9] Michael Tsay, et al., Integrated testing of iodine BIT-3 RF ion propulsion system for 6 U CubeSat applications, Proceedings of the 35th International Electric Propulsion Conference, Atlanta, Georgia, Logan, USA, 2017.
[10] Yongjie Ding, et al., 200 W Hall thruster with hollow indented anode, Acta Astronaut. 139 (2017) 521–527.
[11] Aoyagi Junichiro, et al., Total impulse improvement of coaxial pulsed plasma thruster for small satellite, Vacuum 83 (1) (2008) 72–76.
[12] D. Williams, Propulsion solutions for CubeSats and applications, Proceedings of the CubeSat Developer Workshop, Logan, UT, 2012.
[13] Nembo Buldrin, et al., Small sat propulsion developments at FHWN and FOTEC, Proceedings of the International Workshop in Micropropulsion and CubeSats, Bari, Italy, 2017.
[14] Paige E. Northway, et al., Pulsed plasma thruster gains in specific thrust for CubeSat propulsion, Proceedings of the 53rd AIAA/SAE/ASEE Joint Propulsion Conference, Atlanta, GA, USA, 2017.
[15] Hang Li, et al., A model for macro-performances applied to low power coaxial pulsed plasma thrusters, Acta Astronaut. 170 (2020) 154–162.
[16] D.J. Palumbo, W.J. Guman, Effects of propellant and electrode geometry on pulsed ablative plasma thruster performance, J. Spacecraft 13 (3) (1976) 163–167.
[17] Lei Yang, et al., Study on the wall ablation of heated compound-materials into discharge plasmas based on a modified model, Appl. Phys. Lett. 104 (2014) 084102.
[18] Linghan Zeng, et al., A new ablation model for ablative pulsed plasma thrusters, Acta Astronaut. 160 (2019) 317–322.
[19] Michael Keidar, et al., Analyses of Teflon surface charring and near field plume of a micro-pulsed plasma thruster, Proceedings of the 27th International Electric Propulsion Conference, Worthington, OH, USA, 2001.
[20] Erik L. Antonsen, et al., Effects of postpulse surface temperature on micropulsed plasma thruster operation, J. Propul. Power 21 (5) (2005) 877–883.
[21] Gregory G. Spanjers, et al., P AFRL MicroPPT development for small spacecraft propulsion, Proceedings of the 38th AIAA/SAE/ASEE Joint Propulsion Conference, Indianapolis, Indiana, USA, 2002.
[22] Michael Keidar, et al., Optimization issues for a micropulsed plasma thruster, J. Propul. Power 22 (1) (2006) 48–56.
[23] Michael Keidar, et al., Progress in development of modeling capabilities for a micro-pulsed plasma thruster, Proceedings of the 39th AIAA/SAE/ASEE Joint Propulsion Conference, Huntsville, Alabama, USA, 2003.
[24] Robert G. Jahn, Physics of Electric Propulsion, McGraw-Hill, Inc, New York, 1968 [(Chapter 9)].
[25] Tiankun Huang, et al., Modeling of gas ionization and plasma flow in ablative pulsed plasma thrusters, Acta Astronaut. 129 (2016) 309–315.
[26] Guorui Sun, Zhiwen Wu, Ignition mechanism in ablative pulsed plasma thrusters with coaxial semiconductor spark plugs, Acta Astronaut. 151 (2018) 120–124.
[27] N.N. Smirnov, et al., Accumulation of errors in numerical simulations of chemically reacting gas dynamics, Acta Astronaut. 117 (2015) 338–355.
[28] N.N. Smirnov, et al., Hydrogen fuel rocket engines simulation using LOGOS code, Int. J. Hydrogen Energy 39 (2014) 10748–10756.